Case Studies in Construction Materials 21 (2024) e03947

Contents lists available at ScienceDirect

Case Studies in Construction Materials

journal homepage: www.elsevier.com/locate/cscm

Experimental and theoretical study on flexural performance of lightweight sandwich panels using FRP connectors

Nengming CHENG [a], Juntian TANG [b,*], Peng FENG [b], Zhihao HAO [b], Yaolin ZHANG [a], Mingyuan CHANG [a]

[a] China Construction Science and Industry Corporation Ltd., Shanghai, China
[b] Department of Civil Engineering, Tsinghua University, Beijing, China

ARTICLE INFO

Keywords:
Textile reinforced mortar
FRP pultruded profiles
Flexural test
Analytic model
Comparative analysis
Lightweight sandwich panels

ABSTRACT

Prefabricated concrete sandwich panels are crucial components in the construction of prefabricated buildings, providing essential functions such as load-bearing capacity, thermal insulation, and fire resistance. The development of sandwich panels is oriented toward achieving lightweight, high-strength structures with superior thermal insulation properties. This study introduces two types of innovative sandwich panels using TRM rib with FRP composite bolts and FRP pultruded profiles as connectors, respectively. Comprehensive experiments were conducted to evaluate their construction methods and flexural performance with different thicknesses (i.e., 100 mm and 150 mm). The test results indicate that the proposed sandwich panels can be fabricated in large dimensions of 4 m × 3 m and can withstand substantial equivalent wind loads. The different sandwich panels exhibited distinct failure modes and various composite actions of 8.04 %, 28.36 %, 49.56 %, and 85.67 %. Subsequently, this work presents a theoretical analysis model for predicting the initial stiffness, which has achieved favorable accuracy. Comparative analysis with other studies indicates that the sandwich panels investigated are classified as lightweight, high-strength and thin sandwich panels, which demonstrate significant potential for practical applications.

1. Introduction

In recent years, Precast Concrete Sandwich Panels (PCSPs) have garnered extensive research and interest due to their superior mechanical and thermal insulation properties[1,2]. PCSPs are primarily constructed of concrete or mortar wythes, a middle insulation, and connectors. The exterior and interior wythes, combined by the connectors, primarily bear the structural loads, while the middle insulation serves the functional purposes of thermal insulation, sound insulation, etc.

Over the past two decades, a wide variety of concrete or mortar wythes, insulation, and connectors for PCSPs have been extensively researched. Researchers have used geopolymer concrete[3], reinforced concrete[4], ultra-high performance concrete[5], textile reinforced concrete[6], and glass fiber reinforced concrete[7] as the concrete wythe materials for PCSPs, designing and studying their mechanical properties. For insulation materials, which primarily aim at thermal insulation and sound insulation, materials such as Extruded Polystyrene (XPS), Expanded Polystyrene (EPS) and Polyurethane (PUR) are commonly used[8]. As for connectors, they are research hotspots in PCSPs, with existing studies investigating a range of connectors including concrete ribs[9], steel plates, steel

* Corresponding author.
E-mail address: tjt21@mails.tsinghua.edu.cn (J. TANG).

https://doi.org/10.1016/j.cscm.2024.e03947
Received 1 October 2024; Received in revised form 22 October 2024; Accepted 3 November 2024
Available online 4 November 2024
2214-5095/

meshes, and steel sleeves[10]. However, both steel connectors and concrete ribs can create thermal bridges, reducing the thermal insulation performance. To address this, researchers have also studied FRP rods[11,12], FRP plates[13], and FRP tubes[14] with lower thermal conductivity as connectors. Currently, the research on existing PCSPs is extensive, but there are some issues, such as the thickness of PCSPs commonly around 300 mm, which leads to a higher self-weight, making transportation and installation difficult[2]. Thin panels have both commercial and environmental benefits as a result of material and space savings, but they pose structural challenges as they must resist the same wind loads.

Textile Reinforced Mortar (TRM) and Fiber Reinforced Polymer (FRP) are ideal materials for developing lightweight, high performance thin sandwich panels. TRM consists mainly of cement mortar and FRP textile[15,16], and its post-cracking stiffness and ductility are significantly enhanced by FRP textile. FRP composites are high-performance materials composed of fibers and resin matrix. The strength of Glass Fiber Reinforced Polymer (GFRP) is comparable to that of steel, yet it weighs only one-sixth as much[17]. The thermal conductivity is a quarter that of concrete and one percent that of steel, also with superior corrosion resistance and favorable environmental performance[18]. Given these numerous advantages, this work has developed two types of lightweight sandwich panels using GFRP and TRM.

In terms of theoretical calculations for PCSPs, some scholars have proposed calculation methods. In 2008, a calculation method for sandwich panels was proposed by Li et al.[19], which considered the shear deformation of steel mesh connectors and compared it with finite element results to verify the reliability of the calculations. Bai et al.[20] reviewed two calculation methods for foam concrete sandwich panels, pointed out the unreasonableness of the continuous shear stiffness assumption, and proposed a numerical calculation method that discretizes the connectors. Huang[21] proposed a calculation method considering both flexural deformations of wythes and shear deformations of connectors in his doctoral thesis. Overall, current calculation methods for PCSPs are still under-researched, particularly for thin panels using multiple types of connectors simultaneously.

To reduce the excessive self-weight in existing sandwich panels, this paper proposes two lightweight sandwich panels: one being the TRM sandwich panel and the other the FRP keel sandwich panel. Bending tests have confirmed that both types of panels present good load-bearing capacity. Additionally, this paper conducts a theoretical analysis, distinguishing continuous and discrete connectors, and considers the shear and bending deformations of connectors. A general theoretical analysis method for sandwich panels is derived and its accuracy is verified. Finally, by comparing the bending performance and self-weight of other composite panels, the advancement of this research is demonstrated, along with directions for future research.

2. Experiments

2.1. Specimens

2.1.1. TRM sandwich panel

The TRM Sandwich Panel (TRM-SP) is configured with exterior and interior TRM panels encasing an extruded polystyrene (XPS) layer, connected by GFRP composite bolts. The XPS, produced by extruding polystyrene resin with a foaming agent, is selected for its superior thermal insulation and moisture resistance, which guarantees consistent thermal and mechanical performance even under humid environmental conditions. GFRP connectors are one of the commonly used non-metallic connectors in existing composite sandwich panels[22,23], contribute to reducing the self-weight, enhancing its load-bearing capability, and mitigating thermal bridging, all while being maintenance-free. Nevertheless, existing connectors are generally suitable for concrete panels with a minimum thickness of 200 mm and necessitate an extended anchorage length, which complicates their direct application to the 100 mm to 150 mm thick sandwich panels examined herein. Consequently, this investigation utilized GFRP composite bolts instead of conventional GFRP connectors, with a diameter of 20 mm and an inter-bolt spacing of 500 mm.

The exterior TRM wythe provides superior resistance to bending, cracking, and fatigue, owing to the uniform distribution of GFRP textile within the mortar. GFRP textile was chosen to reduce costs, and polypropylene fibers (PP fibers) were added to further enhance the structural performance of the TRM. The detailed construction process for the TRM-SP is shown in Fig. 1. First, the formwork is laid out according to the design, with key positions such as lifting holes pre-marked. Then, the GFRP combination bolts are placed. Next, the TRM layers are applied step by step. A layer of cement mortar is evenly poured to the specified thickness, followed by the

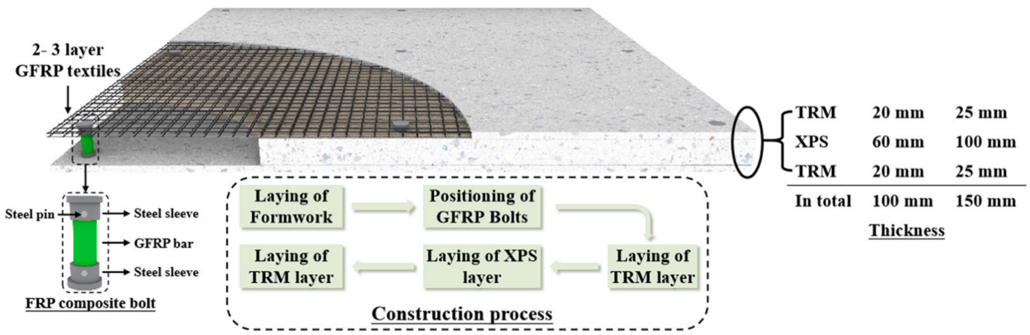

Fig. 1. Construction scheme and construction process of TRM sandwich panels.

placement of a fiber mesh. The mesh is rolled to ensure tight bonding with the mortar. This process is repeated until the required thickness of the TRM layer is achieved. Afterward, the XPS insulation layer is installed, followed by additional TRM layers, again applied in the same manner to reach the designed thickness. Care is taken throughout the process to avoid contact or damage to the already placed bolts. Once the construction is complete, the panel is moved to a designated environment for curing, ensuring that the materials fully harden and reach the specified strength. The GFRP combination bolts run through the entire panel during the construction process. To maintain a clean appearance, the tops of the bolts are embedded into the TRM layer, flush with the surface of the panel. Additionally, to prevent the edges of the insulation material from being exposed to the external environment, a 25 mm layer of cement mortar is poured around the perimeter of the panel to form a protective edge.

2.1.2. FRP keel sandwich panel

The FRP Keel Sandwich Panel (FRP-KSP) consists of TRM panels, FRP keel, XPS, structural adhesive, and self-tapping screws for connections. For the FRP keel, GFRP is selected due to its low cost, high strength-to-weight ratio, corrosion resistance, and low thermal conductivity.

The assembly process for the FRP-KSP is as shown in Fig. 2. First, the FRP keel frame is assembled. The flange ends of the pultruded profiles are cut and then connected using angle steel and bolts. XPS boards are inserted between the FRP keels. Next, the FRP keel is bonded to the TRM panels with epoxy resin adhesive and secured using self-tapping screws. The TRM panels are constructed using the abovementioned method, and structural adhesive is applied to bond the FRP keel to the TRM panels. Screws are inserted at specified points to ensure stability. Once the adhesive has cured, the assembly is flipped, and the process is repeated on the other side. The structural adhesive is applied only between the FRP keel and TRM panels, while self-tapping screws are used to ensure effective bonding performance.

2.1.3. Dimensional properties of specimens

To assess the overall flexural performance of the composite wall panels, four specimens measuring 4000 mm × 3000 mm were prepared in accordance with GB/T 30100–2013[26]. These included two TRM-SP panels, with thicknesses of 100 mm and 150 mm, and two FRP-KSP panels, also with thicknesses of 100 mm and 150 mm. The detailed construction of these composite wall panels is illustrated in Fig. 1, and the specific dimensions of the specimens are provided in Table 1. For identification, each specimen is labeled with "TRM" or "FRP" to indicate the type of panel (TRM-SP or FRP-KSP), followed by a number representing the thickness.

2.2. Material properties

The mix proportions of TRM used in this study are shown in Table 2. In the initial trials, glass fiber was used, but it was observed that glass fiber tended to clump together during mixing, resulting in poor workability of the cement mortar, making construction difficult. Therefore, PP fibers were adopted for subsequent experiments. Both coarse and fine PP fibers are used in conjunction with GFRP textiles. The coarse PP fibers and GFRP textiles primarily contribute to load-bearing, enhancing the tensile strength of the TRM, while the fine PP fibers effectively suppress crack propagation[15,27]. The density of PP fiber is approximately 900 kg/m^3. In this study, 1.0 % coarse PP fiber and 0.1 % fine PP fiber (by volume) are incorporated into the mix. Fig. 3

Three 100 mm × 100 mm × 100 mm cubic specimens were prepared for compression test in accordance with GB/T 50081–2019 [24] with a loading rate of 5 kN/s (i.e., 0.5 MPa/s). These specimens contained only coarse and fine PP fibers and did not include GFRP textiles. The average compressive strength of the specimens was 42.98 MPa.

The compressive, tensile and flexural strengths of the TRM panels with glass fiber mesh were tested in accordance with GB/T 15231–2023[25]. Compressive and tensile tests were conducted using the direct compressive and tensile method, with twelve specimens (30 mm × 30 mm) for compression and twelve specimens (250 mm × 40 mm) for tension. Half of the specimens contain two layers of GFRP textiles and the other half contains three layers of GFRP textiles. Flexural tests were performed using the four-point

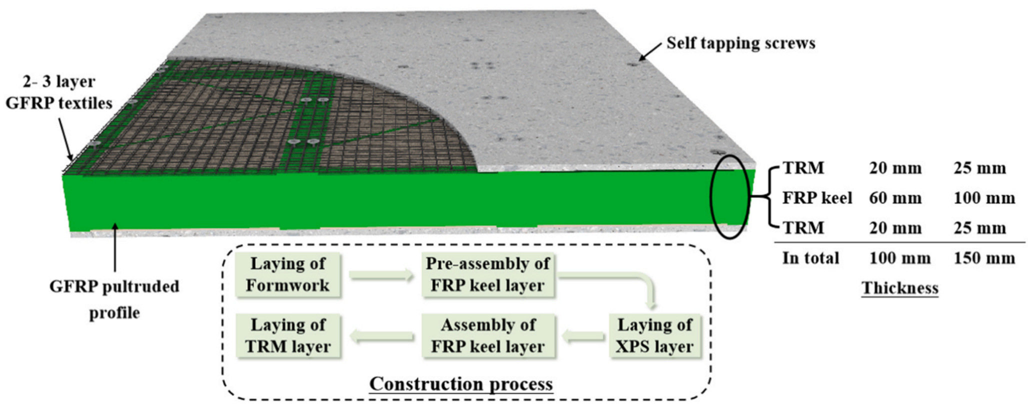

Fig. 2. Construction scheme and construction process of FRP keel sandwich panels.

Table 1
Specimen details.

Specimen	Width (mm)	Length (mm)	thickness(mm)			Connectors
			Exterior wythe	Insulation	Interior wythe	
TRM−100	3000	4000	20	60	20	TRM rib and FRP composite bolts
TRM−150	3000	4000	25	100	25	
FRP−100	3000	4000	20	60	20	FRP pultruded profiles
FRP−150	3000	4000	25	100	25	

Table 2
The mix proportions of TRM (per cubic meter).

P.O 42.5 cement	Sand	Water	Coarse PP Fiber	Fine PP Fiber	Silica fume *	Superplasticizer
650 kg	1215 kg	230 kg	9 kg	0.9	65 kg	15.37 kg

*The silica fume has a fineness of 800 mesh reported by the manufacturer.

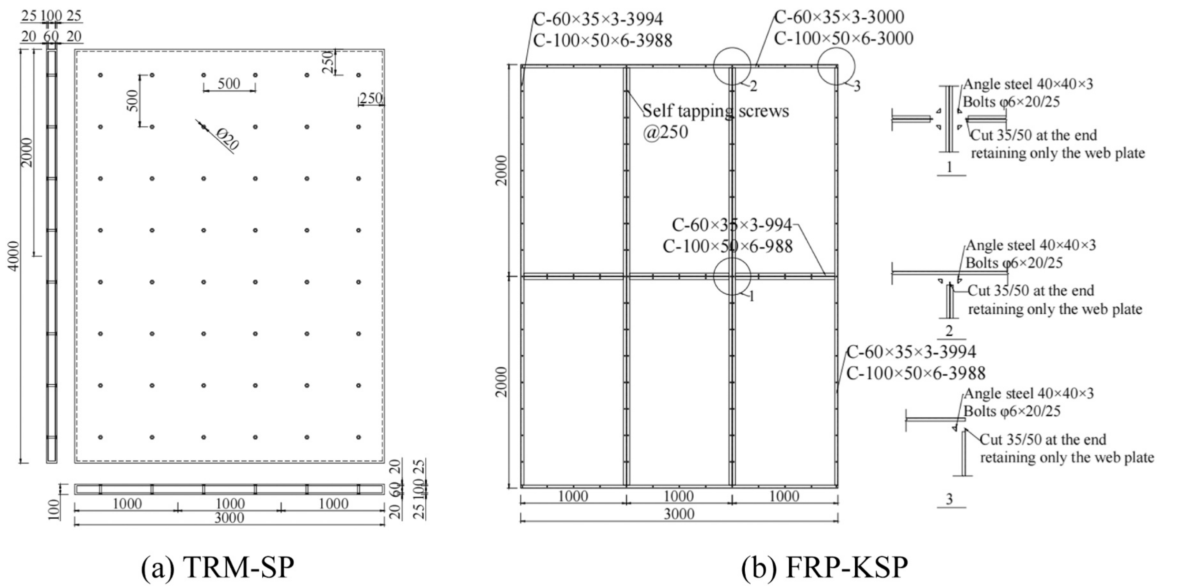

Fig. 3. Schematic of TRM sandwich panels and FRP keel sandwich panels.

bending method for TRM panels, with six specimens (250 mm × 30 mm) for both two-layer and three-layer mesh configurations, respectively. The results are presented in Table 3.

2.3. Test setups and instrumentation

The flexural test setup is shown in Fig. 4, according to GB/T 30100–2013[26]. The test employed a six-point bending test for large-scale TRM-SPs and FRP-KSPs, which, through multi-stage load distribution, can be considered equivalent to a uniform load mode. Steel plates and steel tubes are used to distribute the load. Six strain gauges are arranged on the upper and lower parts of the middle section of the composite wall panel, and four strain gauges are placed on the side of the wall panel to verify the assumption of a

Table 3
Material properties of TRM panels.

Types of tests	Two-layer TRM	Three-layer TRM
Compressive strength (MPa)	56.77	54.24
Tensile strength (MPa)	5.25	6.68
Flexural yield strength (MPa)	9.49	9.87
Ultimate yield strength (MPa)	18.18	22.59
Flexural modulus (MPa)	17879	18156

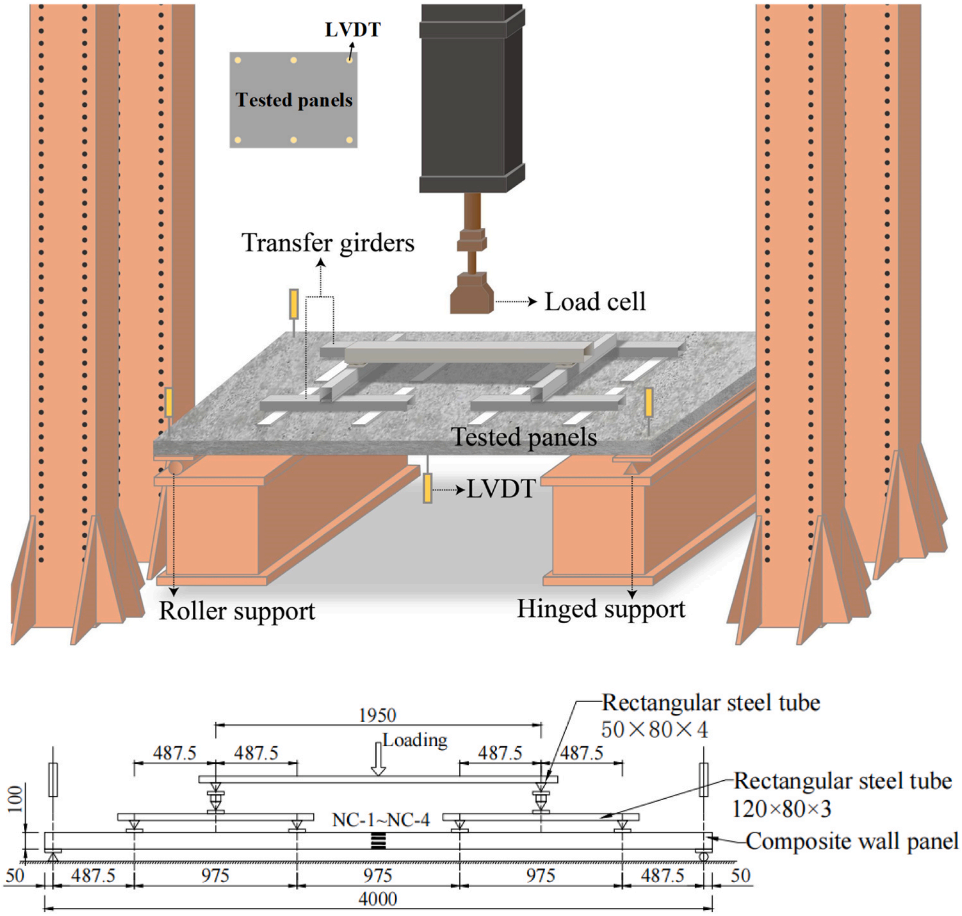

Fig. 4. Setups for flexural test.

plane section. To measure the deflection of the panels and the potential settlement of supports, a total of six LVDTs are installed at the midspan and supports. During the test, the loading rate is maintained at approximately 2.0 kN/min. After the bottom concrete cracks and the stiffness of the composite wall panel degrades, the loading criterion switches to displacement control, maintaining a loading speed of 0.2–0.5 mm/min. The test is ended when the load-bearing capacity of the wall panel drops to 85 % of its maximum capacity.

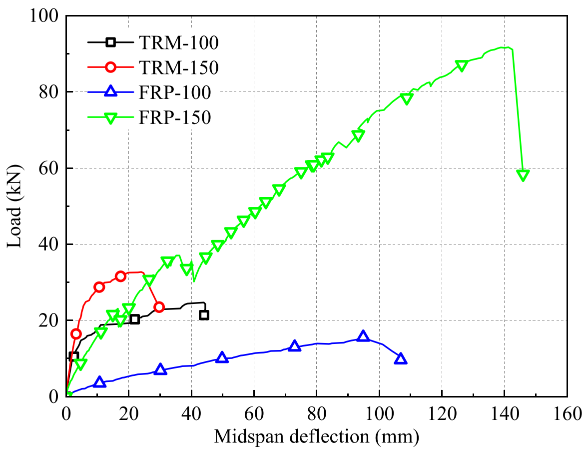

Fig. 5. Load-midspan displacement curves of the flexural test.

2.4. Test results

2.4.1. Load-midspan displacement curves

The load-midspan displacement curves for each specimen are shown in Fig. 5. It can be seen that the slopes of the curves for TRM-SPs are steeper, indicating that the flexural stiffness of the TRM-SPs is generally greater than that of the FRP-KSPs. However, the larger ultimate displacement observed in FRP-KSPs suggests that these panels exhibit better ductility compared to the TRM-SPs.

Both the 100 mm and 150 mm TRM-SPs displayed similar loading behavior, which can be divided into three stages: elastic, yielding, and descending. In the elastic stage, as the load increased, the mid-span displacement of the wall panels increased linearly. The yielding stage followed, where nonlinear deformation began, indicating the material had entered the plastic phase, with cracks appearing and propagating. Finally, in the descending stage, as the load continued to increase, the load-bearing capacity of the panels decreased until failure occurred.

In comparison, the behavior of the 100 mm and 150 mm FRP-KSPs was different. The peak load for the 100 mm FRP-KSP was only 15.99 kN, indicating that the combination effect between the TRM panel and the FRP keel was not realized. This is due to the thinner channel section (C 60×35×3 mm, meaning the channel section with a height of 60 mm, a width of 35 mm and a thickness of 3 mm) used in the 100 mm FRP keel panel. The peak load for the 150 mm FRP-KSP was significantly increased, demonstrating an effective combination effect between the FRP keel and the TRM panel, attributable to a thicker channel section (C 100×50×6 mm, meaning the channel section with a height of 100 mm, a width of 50 mm and a thickness of 6 mm) used in the 150 mm FRP-KSP. In the early stages of loading, both the TRM panels and the FRP keel carry the load. After the TRM panels crack, both components continue to support substantial loads until failure.

2.4.2. Strain analysis

To analyze the development of strain with increasing load, strain from the upper and lower surfaces of the mid-span cross-section of the panels was collected. The load-strain curves of the flexural test are shown in Fig. 6. During the initial stage, the strain in TRM-SPs changes linearly. As the load increases, cracking occurs in the lower TRM panels, leading to stress redistribution and a significant decrease in the stiffness of the components. Consequently, strain gauges in the tension zone are progressively damaged, while the compression zone carries greater stress, causing the strain in the compression zone to exhibit non-linear growth. The strain development trends of the 100 mm and 150 mm sandwich panels are essentially consistent. For FRP-KSPs, after the lower TRM panel fails, the strain in the 150 mm FRP-KSP continues to increase rapidly until a sudden drop occurs, coinciding with the failure of both the panel and the FRP keel. This indicates that the embedded FRP keel carries a substantial load after the TRM panel cracks, leading to a second linear growth phase, which is evident in the load-displacement curve. For the 100 mm FRP-KSP, no second linear growth stage is observed after the lower TRM panel cracks. This is attributed to the smaller cross-section, thinner walls, and lower interface strength of the FRP keel, resulting in immediate failure after cracking of the lower TRM panel.

The strain distribution along the cross-sectional height of the panels is shown in Fig. 7. Before concrete cracking, the strain across the section was relatively small, and the specimens primarily behaved as a unified structure, adhering to the plane section assumption. For the FRP-KSPs, the overall stiffness is relatively weaker due to the low shear stiffness of the core layer, causing the strain distribution to slightly deviate from the plane section assumption. After cracking, the bottom of the specimen fractures, leading to the failure of the strain gauges at the bottom. Despite this, it is still evident that the neutral axis of bending shifts upward, and the strain distribution no longer conforms to the plane section assumption. However, due to the high ductility of the TRM material, the panels continue to exhibit good load-bearing capacity.

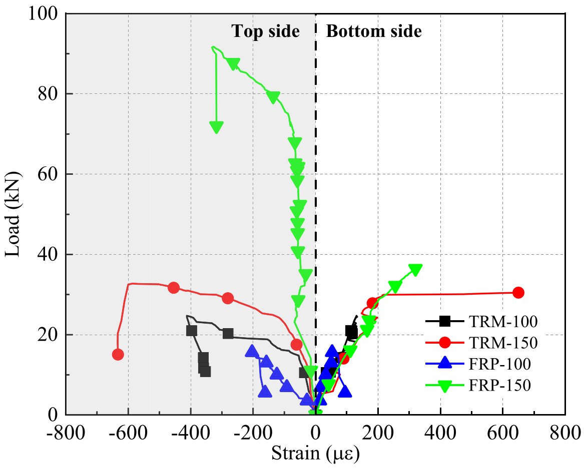

Fig. 6. Load-strain curves of the flexural test.

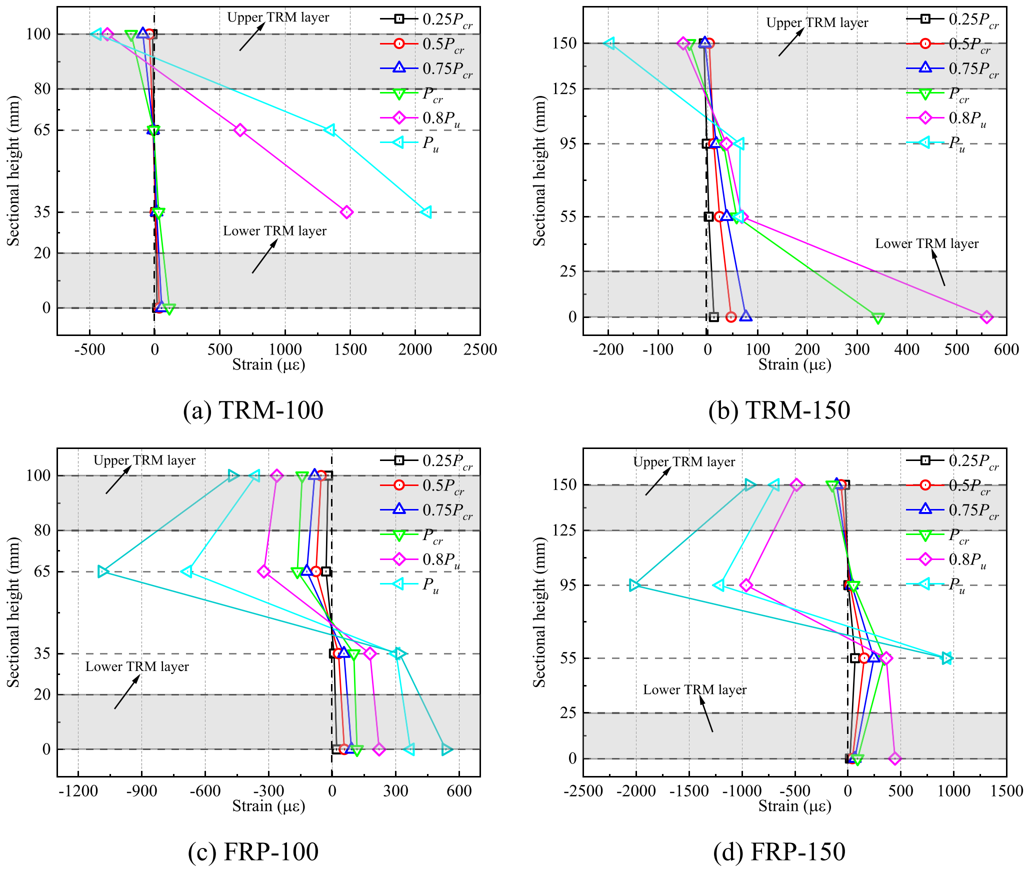

Fig. 7. Strain distribution along the cross-sectional height of the panels.

2.4.3. Failure modes

Fig. 8 presents the failure modes of the specimens. It shows that the failure modes of the TRM-SPs were generally consistent. In the initial stage, the TRM-SP carries the load as a whole until the lower TRM wythe cracks. After cracking, the structural stiffness decreases, with the lower TRM wythe still carrying some load, followed by the appearance of multiple cracks. At failure, lower TRM wythe is riddled with cracks, and tensile failure of the GFRP textiles can be observed at cracks.

In contrast, the failure modes of the FRP-KSPs were different. For the 100 mm FRP-KSP, after the cracking of the lower TRM layer, interlaminar shear failure occurred between the FRP pultruded profiles and the TRM panels. After this, the load was primarily carried by the upper TRM panel and the FRP pultruded profiles. Due to the lower stiffness of the FRP pultruded profiles, they carried a relatively small portion of the load. With the continuous increase in load and displacement, the upper TRM panel ultimately failed. For the 150 mm FRP-KSP, the initial stages of the failure process were similar to those of the 100 mm FRP-KSP, but the load redistribution was different. The higher stiffness of the 150 mm FRP keel allowed it to carry more load, leading to compression failure at the final stage, as shown in Fig. 8.

2.4.4. Flexural performance indicators

In tests, TRM cracking indicates a reduction in structural stiffness leading to the yield of the specimens. The yield point is identified by the farthest point method [28], and it is the point on the load-displacement curve where the curvature matches the secant slope of the peak point (the farthest point), providing a good estimate of the yield point for complex curves. The ductility coefficient is the ratio of the displacement corresponding to the peak load (P_u) to the displacement corresponding to the yield load (P_y). Additionally, polynomial numerical fitting is applied to the loading data before cracking to determine the initial stiffness of the panel. The results are shown in Table 4.

It is evident that the thickness of the panels significantly improves both the yield and ultimate loads for the specimens. This effect is particularly pronounced for the FRP-KSPs. The FRP-KSPs exhibits greater cracking and ultimate displacements compared to the TRM-SPs, because of the outstanding deformation capacity. The initial stiffness of the TRM-SPs is generally superior to that of the FRP-KSPs, highlighting a better combination effect. All tested panels have a ductility coefficient greater than 3.0, classifying them as highly ductile panels.

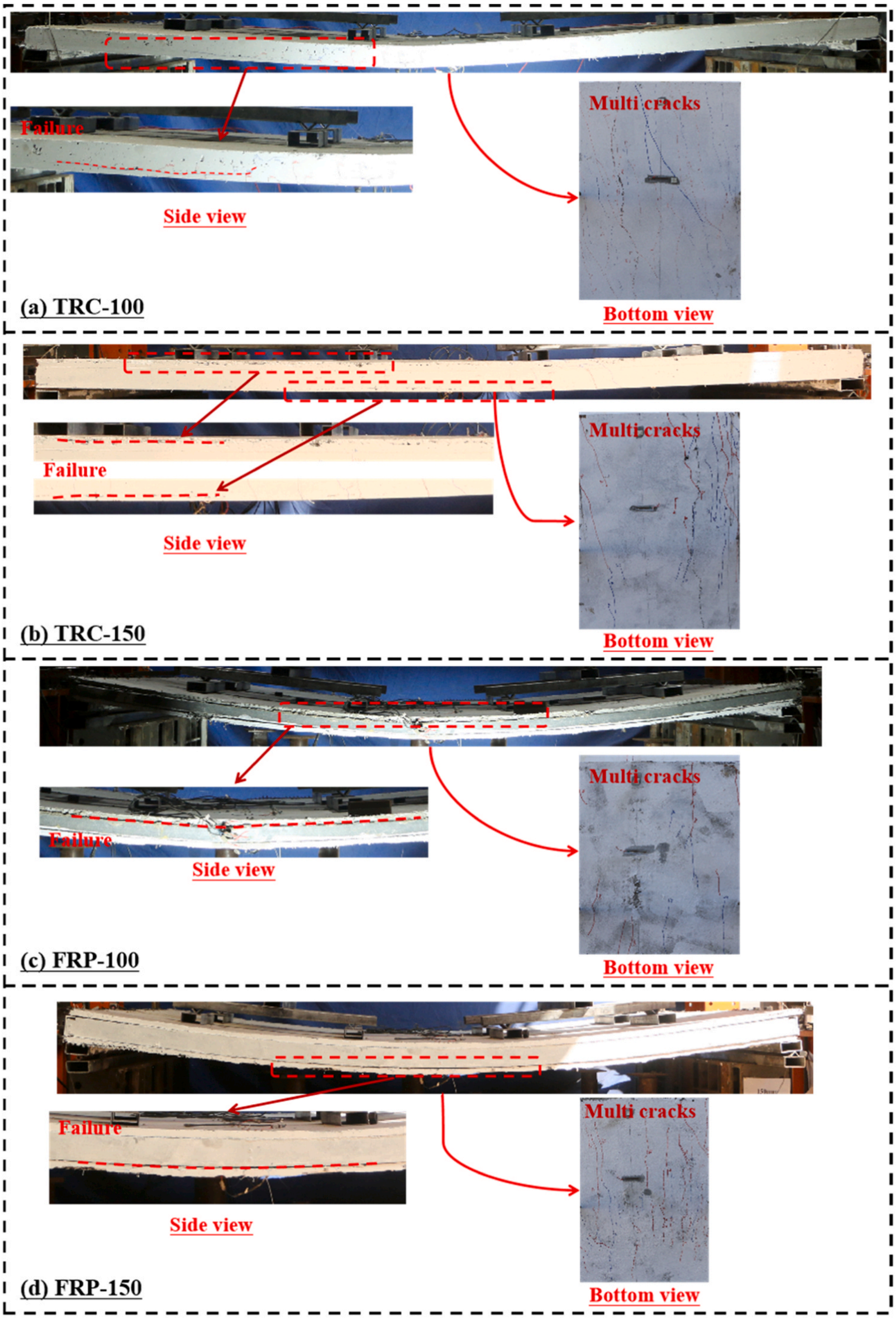

Fig. 8. Failure modes of flexural specimens.

3. Evaluation

3.1. Performance evaluation

The loads at both serviceability and ultimate limit states for the specimens are shown in Table 5. First, the weight of the specimens and loading devices was measured using a weighing machine with a precision of 0.1 kN (100 kg). Under the serviceability limit state, the load on the panel at $l/250$ deflection was taken as the equivalent wind load according to the design requirements. Since this

Table 4
Characteristic points on the load-displacement curves.

Specimens	Yield point		Ultimate point		Initial stiffness	Ductility coefficient
	P_y/(kN)	Δ_y/(mm)	P_u/(kN)	Δ_u/(mm)	S/(kN/mm)	$\mu=\Delta_u/\Delta_y$
TRM−100	16.00	6.77	24.71	44.01	3.90	6.50
TRM−150	24.92	6.28	32.73	24.00	7.01	3.82
FRP−100	5.04	18.53	15.99	94.88	0.45	5.12
FRP−150	36.19	37.04	91.74	141.26	1.99	3.81

Table 5
Serviceability and ultimate limit state results of sandwich wall panels.

Specimens	Self-weight load + Device load (kN)	Serviceability limit state		Ultimate limit state	
		Load at $L/250$ (kN)	Equivalent wind load (kN/m^2)	Ultimate load (kN)	Equivalent wind load (kN/m^2)
TRC−100	9.20+2.50	19.08	1.63	24.71	3.11
TRC−150	12.10+2.50	30.95	2.65	32.73	4.05
FRP−100	9.50+2.50	4.48	0.38	15.99	2.39
FRP−150	12.10+2.50	23.12	1.98	91.74	9.09

deformation was solely caused by external loads, the self-weight of the panels and the weight of the loading devices were not considered in this calculation. In the ultimate limit state, the load-bearing capacity of the panels must account for both their self-weight and the weight of the loading devices. For the flexural test, the equivalent load-bearing area of the panel was considered to be 3 m × 3.9 m. The equivalent wind load was assumed to be a uniformly distributed load, while the six-point bending test also can be considered equivalent to a uniformly distributed load mode.

Table 5 shows that for tested panels in the flexural test, the load-bearing capacities of TRM-100, TRM-150, and FRP-150 in the serviceability limit state are high, at 1.63 kN/m^2, 2.65 kN/m^2, and 1.98 kN/m^2, respectively. These capacities are sufficient to meet the design requirements of typical buildings. However, the load-bearing capacity of FRP-100 is relatively low. In the ultimate limit state, the TRC-SPs show high load-bearing capacities of 3.11 kN/m^2 and 4.05 kN/m^2, while the FRP-KSPs exhibit a significant variation in capacity, with values of 2.39 kN/m^2 and 9.09 kN/m^2.

3.2. Comparative evaluation

To validate the lightweight and high performance of the panels, this study collected data on the self-weight, thickness, and load-bearing capacity of some sandwich panels in reported literature with a thickness of less than 200 mm. The comparative results are illustrated in Fig. 9. The self-weight of the panels was calculated based on the thickness and density of each layer, using density data for common materials[2,8,32]: UHPC and RC were assigned a density of 2500 kg/m^3, GRC a density of 2200 kg/m^3, and the core layer materials EPS and PUR densities of 40 kg/m^3 and 50 kg/m^3, respectively, while the contribution of connectors to the self-weight was neglected. The thickness, weight and load-bearing capacity of thin sandwich panels in existing literature are listed in Table 6.

Fig. 9 demonstrates that the panels in this study present low self-weight, reduced thickness, and considerable yield and ultimate loads, exhibiting certain advancements compared to existing panels. Some sandwich panels exhibited superior mechanical properties,

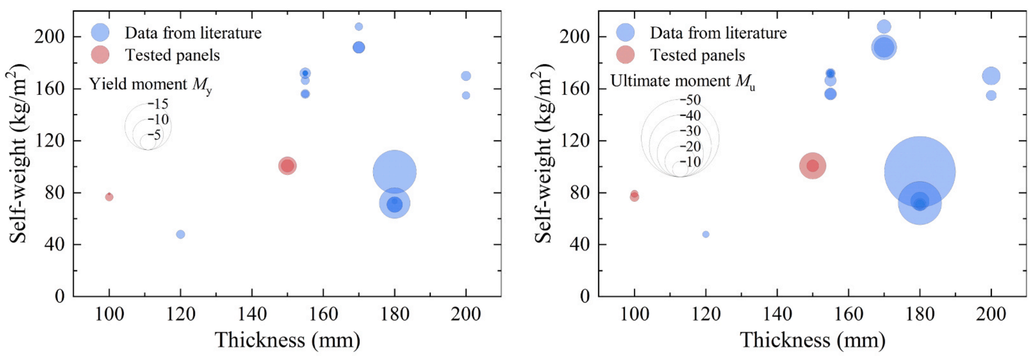

(a) Relationship between self-weight, thickness and yield moment

(b) Relationship between self-weight, thickness and ultimate moment

Fig. 9. Comparison results of sandwich panels.

Table 6
Thickness, weight and load-bearing capacity of thin sandwich panels.

Sources	Thinckness (mm)	Self-weight (kg/m^2)	Yield moment M_y (kNm)	Ultimate moment M_u (kNm)
TRC−100	100	76.67	2.60	5.92
TRC−150	150	100.83	4.05	7.69
FRP−100	100	79.17	0.82	4.55
FRP−150	150	100.83	5.88	17.28
Colombo [29]	120	48.00	2.80	4.32
Flansbjer [31]	200	155.00	2.50	6.70
	200	170.00	3.10	11.80
O'Hegarty [5]	155	166.50	2.70	7.50
O'Hegarty [2]	180	73.50	1.70	12.10
	180	70.80	5.00	8.00
	180	70.80	5.00	6.00
	180	96.00	14.00	46.00
	180	72.00	10.00	28.10
O'Hegarty [30]	155	172.00	1.68	2.61
	155	172.00	1.68	1.77
	155	172.00	1.59	4.95
	155	172.00	1.77	4.57
	155	172.00	3.55	6.07
	170	208.00	2.61	8.77
	155	156.00	2.99	7.19
	155	156.00	2.33	7.75
	170	192.00	3.83	12.69
	170	192.00	3.64	16.52

suggesting that there is potential for further improvement of the panels investigated in this study.

4. Theoretical analysis

4.1. Calculation assumption

When calculating the forces in PCSPs, some assumptions should be considered. Drawing on existing research[19–21,33], the following assumptions have been reasonably considered:

a) Panel deformation assumption: Only the bending deformation of the panels is considered, while axial and shear deformations are ignored, and the wythes have the same curvature when subjected to bending;

b) Connector continuity assumption: Uniformly distributed connectors with rigid ends are used to replace non-uniformly distributed connectors;

c) Connector deformation assumption: Axial deformation of the connectors is neglected, only considering their bending and shear deformations;

d) Insulation assumption: The contribution of the insulation to the strength and stiffness is ignored.

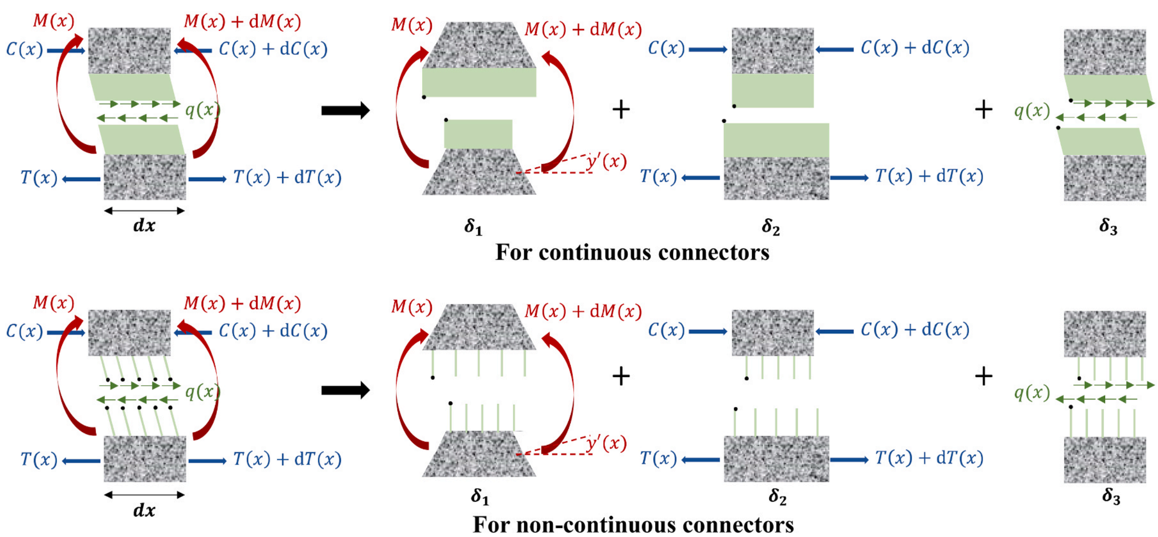

Fig. 10. Deformation analysis model of sandwich panels.

It should be emphasized that this work is the first to consider the bending deformation of connectors, whereas existing literature has only considered their shear deformation, neglecting the bending deformation that dominates for long connectors.

4.2. Analytic model of PCSPs

Conducting an internal force equilibrium analysis on a differential element of the sandwich panel, the forces acting on it are shown in Fig. 10. By performing a force equilibrium analysis on this differential element, the following Eqs. (1)-(3) can be obtained:

$$C(x)+\mathrm{d}C(x)-C(x)=T(x)+\mathrm{d}T(x)-T(x)=q(x)\mathrm{d}x \tag{1}$$

$$M(x)=-EIy''+rC(x) \tag{2}$$

$$EI=E(I_1+I_2) \tag{3}$$

where, $C(x)$, $C(x)$+d$C(x)$, $T(x)$, $T(x)$+d$T(x)$ represent the compressive and tensile force on the two sides of the selected differential element, respectively; $M(x)$ is moment applied on the panel; $q(x)$ is the shear force transmitted through the shear connectors; EI is the flexural stiffness of wythes; y'' is the curvature of panel; E, I_1, and I_2 are the modulus, moment of inertia of exterior and interior wythes, respectively; and r is the neutral axis distance between the exterior and interior wythes.

By performing a deformation analysis at the inflection points of the connectors, it can be determined that they are composed of three parts: the deformation caused by wythes bending δ_1, the deformation caused by the axial tension and compression of the wythes δ_2, and the deformation caused by the bending and shear of the connectors δ_3. According to the assumed conditions, δ_2 can be ignored (δ_2=0), resulting in the following Eqs. (4)-(6):

$$\delta_1+\delta_2+\delta_3=0 \tag{4}$$

$$\delta_1=-ry' \tag{5}$$

$$\delta_3=\frac{q(x)}{K} \tag{6}$$

where, δ_1 is the deformation caused by wythes bending (mm); δ_2 is the deformation caused by the axial tension and compression of the wythes (mm); δ_3 is the deformation caused by the bending and shear of the connectors (mm); y' is the rotation of the panel; K is equivalent shear stiffness of connector (MPa).

Through the above equations, the governing equations for the bending of the sandwich panel can be obtained as Eq. (7). These governing equations have a general solution, as shown in Eqs. (8)-(9). Considering simply supported panels under uniform distributed loads, the solution can be obtained considering the boundary conditions as shown in Eqs. (10)-(11). Further, the shear force distribution and deflection of the panel can be solved as presented in Eqs. (12)-(15):

$$C''(x)-\frac{Kr^2}{EI}C(x)=-\frac{Kr}{EI}M(x) \tag{7}$$

$$C(x)=C_1e^{\lambda x}+C_2e^{-\lambda x}+A(x) \tag{8}$$

$$\lambda^2=\frac{Kr^2}{EI} \tag{9}$$

$$M(x)=\frac{Qx(l-x)}{2} \tag{10}$$

$$C(0)=C(l)=0 \tag{11}$$

$$C(x)=\frac{Q}{\lambda^2r(1+e^{\lambda l})}\left[e^{\lambda x}+e^{\lambda l}e^{-\lambda x}\right]-\frac{Q}{2r}x^2+\frac{Ql}{2r}x-\frac{Q}{\lambda^2 r} \tag{12}$$

$$y(0)=0,\quad y'(0.5l)=0 \tag{13}$$

$$y(x)=\frac{Q}{\lambda^4EI(1+e^{\lambda l})}\left[e^{\lambda x}+e^{\lambda l}e^{-\lambda x}\right]-\frac{Q}{2\lambda^2EI}(x^2-lx+\frac{2}{\lambda^2}) \tag{14}$$

$$y(x)_{\max}=y\left(\frac{l}{2}\right)=-\frac{Q\left(e^{0.5\lambda l}-1\right)^2}{\lambda^4EI(1+e^{\lambda l})}+\frac{Ql^2}{8\lambda^2EI} \tag{15}$$

where, l is the span of the panel (mm); λ is the ratio of equivalent shear stiffness of connector and flexural stiffness of wythes; Q is the uniform load of the panel (N/mm); y is the deflection of the panel (mm).

In the above calculations, it can be observed that r and K are two key parameters to be determined. The r represents the neutral axis distance between the exterior and interior wythes, which is difficult to determine in practical calculations but can be roughly estimated, as shown in Fig. 11. According to the definition of the neutral axis, the following Eq. (16) can be obtained, and the range of y_c can be determined as shown in Eq. (17). When the panel thickness is much greater than the insulation thickness, y_c is closer to 0.67t, and when the panel thickness is much less, y_c is closer to 0.5t, which is line with general understanding. In this study, the panel thickness is less than the insulation thickness, so it is reasonable to take y_c as 0.5t.

$$y_c = \frac{\int_0^h \sigma t \mathrm{d}t}{\int_0^h \sigma \mathrm{d}t} = \frac{\frac{1}{2}\sigma_1 + \frac{1}{3}y'' t^2}{\sigma_1 + \frac{1}{2}y'' t}, \quad t > 0 \tag{16}$$

$$\frac{1}{2}t \leq y_c \leq \frac{2}{3}t \tag{17}$$

where, σ_1 and t are the edge stress and thickness of the exterior or interior layer, respectively; y_c is the distance from the edge to the point of resultant force.

In calculations, K represents the equivalent shear stiffness of the connector. For continuous connectors, only the shear deformation of the connectors is considered, and the equivalent shear stiffness is as shown in Eq. (18). For non-continuous connectors, the bending deformation of the connectors needs to be considered. In this study, the exterior and interior wythes have the same thickness, and the inflection points of the connectors are at the midspan. The deformation caused by the bending and shear of the connectors δ_3 at the deflection points, is shown in Eq. (19), and the equivalent shear stiffness is shown in Eq. (20).

$$K = \frac{\mu G_s A_s}{A}, \text{ for continuous connectors} \tag{18}$$

$$\delta_3 = 2 \times \left(\frac{q(x)d(0.5t_s)^3}{3E_s I_s} + \frac{q(x)d \bullet 0.5t_s}{\mu G_s A_s}\right) \tag{19}$$

$$K = \frac{1}{\frac{dt_s^3}{12E_s I_s} + \frac{dt_s}{\mu G_s A_s}}, \text{ for non-continuous connectors} \tag{20}$$

where, d, t_s, E_s, I_s, G_s, A_s and μ are the spacing, height, Young's modulus, moment of inertia, shear modulus, area and uniformity coefficient of shear force distribution of the connectors, respectively; μ is the uniformity coefficient of shear force distribution of the connectors, which is 1.11 for circle section and 1.20 for rectangle section; A is the area of the panel.

When the connector stiffness is very small or the spacing is very large, i.e., the equivalent shear stiffness K is very small, the mid-span deflection of the simply supported uniform distributed beam can be approximated to that of an uncoupled beam, as shown in Eq. (21). When the connectors stiffness is very large, therefore the equivalent shear stiffness K is very large, the mid-span deflection of the simply supported uniform distributed beam approaches zero, as shown in Eq. (22). This is because that the load is primarily borne by the high-stiffness connectors, resulting in zero deformation of the panels.

$$K \to 0, \lambda \to 0, \quad y\left(\frac{l}{2}\right) = -\frac{Q\left(e^{0.5\lambda l}-1\right)^2}{\lambda^4 EI(1+e^{\lambda l})} + \frac{Ql^2}{8\lambda^2 EI} \to \frac{5}{384}\frac{Ql^4}{EI} \tag{21}$$

$$K \to \infty, \lambda \to \infty, \quad y\left(\frac{l}{2}\right) = -\frac{Q\left(e^{0.5\lambda l}-1\right)^2}{\lambda^4 EI(1+e^{\lambda l})} + \frac{Ql^2}{8\lambda^2 EI} \to 0 \tag{22}$$

If a uniform bending method is employed, the equivalent flexural stiffness of the section can be calculated according to the following Eqs. (23)-(24):

$$I_{test} = \frac{5}{384E}\frac{Ql^4}{y\left(\frac{l}{2}\right)} = \frac{5l^4}{384E}S \tag{23}$$

$$I_{pre} = \frac{5l^4}{384}\frac{I}{-\frac{\left(e^{0.5\lambda l}-1\right)^2}{\lambda^4\left(1+e^{\lambda l}\right)} + \frac{l^2}{8\lambda^2}} \tag{24}$$

where, I_{test}, I_{pre} the equivalent moment of inertia obtained from the experiment and theoretical model, S is the initial stiffness determined by the test, as shown in Table 4.

If a four-point bending method is applied for sandwich panels, the mid-span displacement can be calculated in a manner similar to the one mentioned above, and subsequently, the equivalent flexural stiffness of the section can be determined as Eqs. (25)-(27):

$$y\left(\frac{l}{2}\right) = -\frac{F(e^{\lambda a}-e^{-\lambda a})e^{0.5\lambda l}}{2\lambda^3 EI(1+e^{\lambda l})} + \frac{Fa}{2\lambda^2 EI} \tag{25}$$

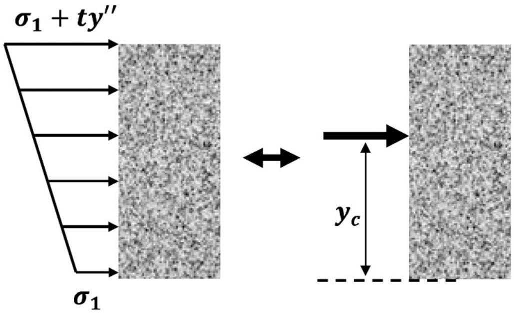

Fig. 11. Calculation of neutral axis of TRM wythe.

$$I_{test} = \frac{(3l^2 - 4a^2)a}{48E} S \tag{26}$$

$$I_{pre} = \frac{(3l^2 - 4a^2)a}{48} \frac{I}{-\frac{(e^{\lambda a} - e^{-\lambda a})e^{0.5\lambda l}}{2\lambda^3(1+e^{\lambda l})} + \frac{a}{2\lambda^2}} \tag{27}$$

where, a is the distance from the load point to the support point.

4.3. Validation

Referencing existing evaluation methods[34–37], the degree of composite action of the sandwich panel is described by Eq. (28). The closer the composite action is to 1.0, the better the exterior and interior wythes work together, resulting in higher stiffness. Conversely, if the composite action is less, they will act independently to bear loads, resulting in lower stiffness.

$$\kappa = \frac{I_{test} - I_{nc}}{I_c - I_{nc}} \tag{28}$$

where, I_c and I_{nc} is the full-composite and non-composite moment of inertia of the panel.

Based on the aforementioned theoretical analysis, the tested and predicted initial stiffness for the four specimens can be determined, as shown in Table 7. It can be observed that the theory provides a good prediction accuracy of the initial stiffness. Additionally, data from existing literature were selected for theoretical validation, also as presented in the table. The validation results indicate that the theory has good applicability to different sandwich panels and various connectors.

5. Discussion

In order to develop lightweight and high performance PCSPs, this work presents two types of lightweight sandwich panels and conducts an in-depth experiment on their flexural behavior. Additionally, a theoretical model is proposed that considers the effects of both continuous and discontinuous connectors in the sandwich panels to predict the initial stiffness of the wall panels. Through comparative analysis, the work validates the theoretical model and the superior performance of the studied sandwich panels.

The two types of panels proposed in this paper are preliminary tests, and their structural configurations require further optimization, such as the arrangement of concrete ribs, the impact of concrete ribs on overall thermal and sound insulation performance, and

Table 7
Validation of analytic model with different connectors.

Sources	Type of connector	K(MPa)	I_{test}(mm^4)	I_{pre}(mm^4)	Error (%)	κ(%)
TRM−100	TRM rib and FRP composite bolts	233.42	1.68×10^8	1.49×10^8	−11.35	85.67
TRM−150		221.73	2.98×10^8	3.09×10^8	3.61	49.56
FRP−100	FRP pultruded profiles	27.69	1.94×10^7	2.10×10^7	8.25	8.04
FRP−150		55.38	8.47×10^7	8.25×10^7	−2.53	28.36
Huang [21]	FRP plate	16.70	3.12×10^7	2.94×10^7	−5.71	5.75
		16.70	3.05×10^7	2.94×10^7	−3.54	5.35
		16.70	3.03×10^7	2.94×10^7	−2.90	5.24
		16.70	3.05×10^7	2.94×10^7	−3.54	5.35
	Hexagonal tube	24.00	3.44×10^7	3.55×10^7	3.24	7.89
		42.00	4.46×10^7	4.59×10^7	2.86	13.08
		24.00	3.51×10^7	3.55×10^7	1.19	7.65
		42.00	4.33×10^7	4.59×10^7	5.95	12.33

the arrangement of FRP keels. Existing tests and analyses have demonstrated their mechanical properties, but further studies, such as thermal insulation, sound insulation, and fire resistance, still need to be pursued, especially for the fire resistance, which is important and of great influence for civil buildings[35,36].

The proposed theoretical model can consider the combined effect of connectors and obtain the initial flexural stiffness of the panels. However, this model struggles to conduct strength analysis of thin panels. This is because that, for the stiffness analysis, it reflects the whole behavior of PCSPs before cracking and can be well analyzed under the given assumptions. However, for the strength analysis, it reflects the local failure behavior caused by stress concentration near the shear connectors, especially for the thin panels with non-uniform connector distribution and high composite action, such as the TRM-100 and TRM-150. As observed in tests, the initial cracks of TRM-100 and TRM-150 primarily occur near the TRM ribs. Therefore, reasonable strength prediction models need to be developed. During the loading process of sandwich panels, the connectors may also fail, or interfacial failure may occur between the connectors and the panel surfaces, leading to poor composite action (evaluated as Eq. (28)) and low stiffness. In this study, interfacial failure between the pultruded profile and the panel surfaces was observed in the FRP-100 and FRP-150. However, due to the poor composite action of the panels, the decrease in stiffness was not significant.

The theoretical model proposed in this study comprehensively considers both the shear and bending deformations of non-continuous connectors. When non-continuous shear connectors are of considerable length, bending deformation cannot be neglected. In this study, for the FRP connectors in TRM-SPs, if only shear deformation is considered as Eq. (20), the equivalent shear stiffness K of the FRP composite bolts is 33.51 MPa for TRM-100 and 20.11 MPa for TRM-150, which differs by 45 % and 145 % from the values of 23.17 MPa and 8.22 MPa, respectively, when bending deformation is taken into account. Therefore, the bending deformation of non-continuous connectors should not be ignored in thin panels.

The study finds that the contribution of appropriate concrete ribs is significantly greater than that of FRP connectors. However, concrete has poor thermal conductivity[37] (about 1.74 W/(m·K)) compared to FRP (about 0.52 W/(m·K)) and insulation (about 0.03 W/(m·K) for XPS), which can easily lead to thermal bridging. Therefore, this research proposes the use of FRP pultruded profiles as continuous connectors, but these are also prone to interfacial damage. Subsequent attempts could involve embedding the FRP pultruded profiles into the panel and casting them together to avoid interfacial failure.

Some of the assumptions within the theoretical model still require refinement. On one hand, the interlayer shear is significantly greater at the ends than in the middle, resulting in a higher contribution from the connectors at the ends and a lesser contribution from those in the middle. On the other hand, when the connectors at the ends experience great deformation[38], shear connectors may yield and rotate, causing them to bear additional tensile loads, which is less considered in existing research, and this contribution is not clear.

6. Conclusions

This study introduces a novel TRM sandwich panel (TRM-SP) and FRP keel sandwich panel (FRP-KSP). The TRM-SP is primarily composed of TRM panels, XPS boards, and GFRP composite bolts. The FRP-KSP mainly consists of TRM panels, XPS boards, and FRP pultruded profile keel. Both panels are suitable for use in common steel-framed prefabricated buildings and offer advantages such as lightweight, high strength, excellent thermal insulation, and significant environmental potential. Their flexural performance was evaluated, leading to some conclusions:

1. The 100 mm and 150 mm TRC-SPs demonstrated load-bearing capacities of 1.63 kN/m^2 and 2.65 kN/m^2 under the serviceability limit state, respectively; and 3.11 kN/m^2 and 4.05 kN/m^2 under ultimate limit state, respectively. The 100 mm and 150 mm FRP-KSPs showed load-bearing capacities of 0.38 kN/m^2 and 1.98 kN/m^2 under the serviceability limit state, respectively; and 2.39 kN/m^2 and 9.09 kN/m^2 under ultimate limit state, respectively. The experimental results indicate that these panels can meet the design requirements of typical buildings.

2. The proposed sandwich panels can achieve different initial stiffness through the connectors and panel thickness. The four specimens tested in this study realized composite action of 8.04 %, 28.36 %, 49.56 %, and 85.67 %, respectively, further validating their design flexibility.

3. An analytical model for sandwich panels is presented in this study, validated with experimental data from this study and existing research, demonstrating its accuracy in predicting the initial flexural stiffness of sandwich panels.

4. By comparing the load-bearing capacity, self-weight, and thickness of sandwich panels from existing studies, this paper confirms that the sandwich panels investigated are lightweight, high-strength, and thin, with promising application prospects.

CRediT authorship contribution statement

Juntian Tang: Writing – review & editing, Writing – original draft, Visualization, Validation, Formal analysis, Data curation, Conceptualization. **Peng FENG:** Supervision, Resources, Project administration, Methodology, Investigation, Funding acquisition, Conceptualization. **Zhihao HAO:** Writing – review & editing, Writing – original draft, Visualization, Data curation. **Yaolin ZHANG:** Supervision, Methodology, Funding acquisition, Conceptualization. **Mingyuan CHANG:** Resources, Project administration, Investigation, Funding acquisition, Conceptualization. **Nengming CHENG:** Supervision, Project administration, Methodology, Investigation, Funding acquisition, Conceptualization.

Declaration of Competing Interest

The authors declare that they have no known competing financial interests or personal relationships that could have appeared to influence the work reported in this paper.

Acknowledgment

This research was supported by the “Study and Application of High-Performance Fiber-Reinforced Composite External Wall Panels and Connection Joints” under grant from China Construction Science and Industry Corporation Ltd.

Data availability

Data will be made available on request.

References

[1] K.E. Seeber, R. Andrews, J.R. Baty, P.S. Campbell, J.E. Dobbs, G. Force, S. Francies, S. Freedman, H.A. Gleich, G.E. Goettsche, D.W. Hanson, P. Hynes, P. J. Iverson, F.J. Jacques, P. Kourajian, State-of-the-art of precast/prestressed sandwich wall panels, PCI J. 42 (2) (1997), https://doi.org/10.15554/pcij42.2-05.
[2] R. O'Hegarty, O. Kinnane, Review of precast concrete sandwich panels and their innovations, Constr. Build. Mater. 233 (2020) 117145, https://doi.org/10.1016/j.conbuildmat.2019.117145.
[3] J.Q. Huang, J.G. Dai, Flexural performance of precast geopolymer concrete sandwich panel enabled by FRP connector, Compos. Struct. 248 (2020) 112563, https://doi.org/10.1016/j.compstruct.2020.112563.
[4] I. Choi, J.H. Kim, Y.C. You, Effect of cyclic loading on composite behavior of insulated concrete sandwich wall panels with GFRP shear connectors, Compos. Part B: Eng. 96 (2016), https://doi.org/10.1016/j.compositesb.2016.04.030.
[5] R. O'Hegarty, R. West, A. Reilly, O. Kinnane, Composite behaviour of fibre-reinforced concrete sandwich panels with FRP shear connectors, Eng. Struct. 198 (2019) 109475, https://doi.org/10.1016/j.engstruct.2019.109475.
[6] N. Williams Portal, M. Flansbjer, K. Zandi, L. Wlasak, K. Malaga, Bending behaviour of novel Textile Reinforced Concrete-foamed concrete (TRC-FC) sandwich elements, Compos. Struct. 177 (2017), https://doi.org/10.1016/j.compstruct.2017.06.051.
[7] A. Enfedaque, D. Cendón, F. Gálvez, V. Sánchez-Gálvez, Failure and impact behavior of facade panels made of glass fiber reinforced cement(GRC), Eng. Fail. Anal. 18 (7) (2011), https://doi.org/10.1016/j.engfailanal.2011.01.004.
[8] H. Tawil, C.G. Tan, N.H.R. Sulong, F.M. Nazri, M.M. Sherif, A. El-Shafie, Mechanical and Thermal Properties of Composite Precast Concrete Sandwich Panels: A Review, Buildings 12 (9) (2022), https://doi.org/10.3390/buildings12091429.
[9] I. Choi, J.H. Kim, H.R. Kim, Composite behavior of insulated concrete sandwich wall panels subjected to wind pressure and suction, Materials 8 (3) (2015), https://doi.org/10.3390/ma8031264.
[10] C. Naito, J. Hoemann, M. Beacraft, B. Bewick, Performance and Characterization of Shear Ties for Use in Insulated Precast Concrete Sandwich Wall Panels, J. Struct. Eng. 138 (1) (2012), https://doi.org/10.1061/(asce)st.1943-541x.0000430.
[11] W. Xue, Y. Li, K. Fu, X. Hu, Y. Li, Accelerated ageing test and durability prediction model for mechanical properties of GFRP connectors in precast concrete sandwich panels, Constr. Build. Mater. 237 (2020) 117632, https://doi.org/10.1016/j.conbuildmat.2019.117632.
[12] J. Yang, W. Xue, X. Li, Mechanical properties test of FRP connectors in precast sandwich insulation wall panels, Jiangsu Daxue Xuebao (Ziran Kexue Ban.)/J. Jiangsu Univ. (Nat. Sci. Ed.) 34 (6) (2013), https://doi.org/10.3969/j.issn.1671-7775.2013.06.019.
[13] A. Chen, T.G. Norris, P.M. Hopkins, M. Yossef, Experimental investigation and finite element analysis of flexural behavior of insulated concrete sandwich panels with FRP plate shear connectors, Eng. Struct. 98 (2015), https://doi.org/10.1016/j.engstruct.2015.04.022.
[14] S. Kumar, B. Chen, Y. Xu, J.G. Dai, Structural behavior of FRP grid reinforced geopolymer concrete sandwich wall panels subjected to concentric axial loading, Compos. Struct. 270 (2021) 114117, https://doi.org/10.1016/j.compstruct.2021.114117.
[15] P. Zhou, P. Feng, Unified analysis for tailorable multi-scale fiber reinforced cementitious composites in tension, Compos. Part B: Eng. 254 (2023) 110586, https://doi.org/10.1016/j.compositesb.2023.110586.
[16] S.M. Raoof, L.N. Koutas, D.A. Bournas, Textile-reinforced mortar (TRM) versus fibre-reinforced polymers (FRP) in flexural strengthening of RC beams, Constr. Build. Mater. 151 (2017), https://doi.org/10.1016/j.conbuildmat.2017.05.023.
[17] P. Feng, Development and application of composite in civil engineering, Compos. Sci. Eng. 09 (2014) 99–104 (in Chinese).
[18] T. Liu, J.-T. Tang, S. Zhang, L. Dong, L. Hu, X. Meng, Y. Zhao, P. Feng, Carbon emissions of durable FRP composite structures in civil engineering, Eng. Struct. 315 (2024) 118482, https://doi.org/10.1016/j.engstruct.2024.118482.
[19] Y.B. Li, S.H. Zhang, B.Y. Xia, Theoretical calculation and analysis of slip and deformation for concrete sandwich panel, Gongcheng Lixue/Eng. Mech. 25 (1) (2008).
[20] F. Bai, J.S. Davidson, Analysis of partially composite foam insulated concrete sandwich structures, Eng. Struct. 91 (2015), https://doi.org/10.1016/j.engstruct.2015.02.033.
[21] Huang, J. (2019). Structural performance of precast reinforced geopolymer concrete sandwich panels enabled by frp connectors. Ph. D thisis, Hong Kong Polytechnic University, Hong Kong, China.
[22] J.Q. Huang, J.G. Dai, Direct shear tests of glass fiber reinforced polymer connectors for use in precast concrete sandwich panels, Compos. Struct. 207 (2019), https://doi.org/10.1016/j.compstruct.2018.09.017.
[23] Q. Huang, E. Hamed, Nonlinear finite element analysis of composite precast concrete sandwich panels made with diagonal FRP bar connectors, Compos. Struct. 212 (2019), https://doi.org/10.1016/j.compstruct.2019.01.019.
[24] GB/T 50081-2019. Standard for test methods of concrete physical and mechanical properties. Beijing China: Ministry of Housing and Urban-Rural Development of the PRC; 2019.
[25] 2023, GB/T 15231, 2003. -Test methods for the properties of glassfibre reinforced cement2023, AQSIQ; SAC, Beijing China..
[26] GB/T 30100 Beijing China AQSIQ;SAC2013.
[27] P. Zhou, P. Feng, J. Qiu, Analysis of the tensile behavior of FRP textile for multi-scale fiber reinforced cementitious composite, Cem. Concr. Compos. 147 (2024), https://doi.org/10.1016/j.cemconcomp.2023.105416.
[28] P. Feng, H. Qiang, L.P. Ye, Discussion and definition on yield points of materials, members and structures, Gongcheng Lixue/Eng. Mech. 34 (2017) 36–46.
[29] I.G. Colombo, M. Colombo, M. di Prisco, Bending behaviour of Textile Reinforced Concrete sandwich beams, Constr. Build. Mater. 95 (2015), https://doi.org/10.1016/j.conbuildmat.2015.07.169.
[30] R. O'Hegarty, O. Kinnane, M. Grimes, J. Newell, M. Clifford, R. West, Development of thin precast concrete sandwich panels: Challenges and outcomes, Constr. Build. Mater. 267 (2021) 120981, https://doi.org/10.1016/j.conbuildmat.2020.120981.
[31] M. Flansbjer, N. Williams Portal, D. Vennetti, U. Mueller, Composite Behaviour of Textile Reinforced Reactive Powder Concrete Sandwich Façade Elements, Int. J. Concr. Struct. Mater. 12 (1) (2018), https://doi.org/10.1186/s40069-018-0301-4.
[32] GB 50009-2012. Load code for the design of building structures. Beijing China, 2012.

[33] Y. Wang, J. Wang, D. Zhao, G. Hota, R. Liang, D. Hui, Flexural Behavior of Insulated Concrete Sandwich Panels using FRP-Jacketed Steel-Composite Connectors, Adv. Mater. Sci. Eng. 2022 (2022), https://doi.org/10.1155/2022/6160841.
[34] A. Chen, M. Yossef, P. Hopkins, A comparative study of different methods to calculate degrees of composite action for insulated concrete sandwich panels, Eng. Struct. 212 (2020) 110423, https://doi.org/10.1016/j.engstruct.2020.110423.
[35] L. Hu, X. Liang, P. Feng, H.T. Li, Temperature effect on buckling behavior of prestressed CFRP-reinforced steel columns, Thin-Walled Struct. 188 (2023), https://doi.org/10.1016/j.tws.2023.110879.
[36] X. Liang, W. Wang, L. Hu, P. Feng, Experimental and numerical study on high-temperature performance of prestressed CFRP-reinforced steel columns, Eng. Struct. 301 (2024), https://doi.org/10.1016/j.engstruct.2023.117347.
[37] GB 50176-2016. Code for thermal design of civil building. Beijing China, 2016.
[38] I. Choi, J.H. Kim, D.W. Kim, J.S. Park, Effects of grid-type shear connector arrangements used for insulated concrete sandwich wall panels with a low aspect ratio, J. Build. Eng. 46 (2022), https://doi.org/10.1016/j.jobe.2021.103754.